

http://pubs.acs.org/journal/aelccp

Prospects for Aerobic Photocatalytic Nitrogen **Fixation**

Yu-Hsuan Liu, Carlos A. Fernández, Sai A. Varanasi, Nhat Nguyen Bui, Likai Song, and Marta C. Hatzell*



Downloaded via GEORGIA INST OF TECHNOLOGY on December 30, 2021 at 16:38:50 (UTC). See https://pubs.acs.org/sharingguidelines for options on how to legitimately share published articles.

Cite This: ACS Energy Lett. 2022, 7, 24-29



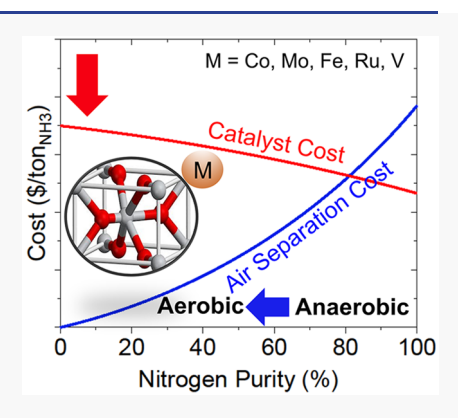
ACCESS

III Metrics & More

Article Recommendations

Supporting Information

ABSTRACT: Decarbonized ammonia production through photocatalytic nitrogen fixation is appealing, as it may allow for farm-scale fertilizer production using earthabundant feedstocks, energy, and catalysts. Yet, the viability of decentralized ammonia production systems is largely dependent on the cost of a complete photocatalytic system reaching a Haber-Bosch parity point. Here, we demonstrate that an air separation unit for a farm-scale low-cost photocatalytic ammonia synthesis system can account for 70% of the total system cost. This high cost depends on the type of air separation unit and the purity of nitrogen. This promotes the need for a catalyst, which can tolerate trace oxygen or can even operate under aerobic conditions to attain Haber-Bosch cost parity. We further demonstrate the change in catalytic activity of prototypical undoped and metal-doped titania photocatalysts under aerobic and anaerobic conditions. Among various metal-doped titania photocatalyst, vanadium- and ruthenium-doped titania demonstrated no performance decline under aerobic conditions.



¶ he synthesis of ammonia has the highest energy consumption (2.5 EJ/yr) and carbon emission (340 Mt CO₂ eq/yr) of any commodity chemical. ¹⁻⁴ The high environmental impact is attributed to the use of steam reforming to produce hydrogen, the production scale (200 Mt NH₃/year), and the energy intensity required to maintain reactor operating conditions (~100 bar and ~700 K). 5,6 This promotes investment in ammonia production facilities that are located centrally and within economically advantaged regions to drive down the cost to 300-400 U.S. dollar $(USD)/t_{NH}$. However, the primary use of ammonia (80%) is for the production of nitrogen-based fertilizers, which are often used in decentralized and economically disadvantaged regions.³ The disconnection between centralized fertilizer production and decentralized fertilizer use has driven the industry to manufacture solid and highly concentrated fertilizers to minimize transportation costs $(Cost_{transp} \approx 50 \text{ USD/t}_{NH_3})$. The manufacture, distribution, and use of highly concentrated fertilizers has resulted in several challenges related to equity, safety, and product access. As such, many farmers in developing countries opt not to apply fertilizer due to the cost, resulting in reduced agricultural yields and livelihood when compared to developed countries.⁸ All these factors have promoted investigations of alternative catalytic systems beyond the Haber-Bosch process, which may be able to democratize access to ammonia-based fertilizers. To accomplish this, a

modular, small-scale reactor capable of operating with renewable energy is essential.

Most investigations aimed at designing modular and electrified ammonia synthesis reactors focus on electrocatalysis, 9-18 plasma-based catalysis, 19,20 mechanocatalysis, 21 and photocatalysis.²² Electrocatalysis occurs within an electrolysis-based architecture driven by a renewable energy source (e.g., solar, wind, hydroelectric, etc.). The critical component within an electrocatalytic reactor is the electrocatalyst. Many demonstrations suggest that noble metals (e.g., Au, Pd, Ru)^{11,14} and transition metals¹⁵ are capable of activating nitrogen in an electrochemical cell. Plasma-based catalysis typically occurs within a reactor vessel where nonequilibrium ionic gas (e.g., plasma) is generated using renewable electricity. In contrast to electrocatalysis, plasma is capable of activating nitrogen without the addition of catalysts and has achieved 100% faradaic efficiencies. 19,20 Mechanocatalysis occurs within a vessel that contains milling balls, a catalyst, and a reactant. Here, mechanical energy is generated using renewable electricity to produce nitrides, which

Received: October 16, 2021 Accepted: November 19, 2021



ultimately result in the formation of ammonia when exposed to hydrogen 21 . Finally, photocatalysis occurs on a particle-based or film-based semiconductor (e.g., slurry-type or photoelectrode). The semiconductor electrode or particle is typically biased by incident solar energy, generating charge carriers that activate nitrogen. The most widely studied catalysts include metal oxides (e.g., ${\rm TiO_2}$, ${\rm BiOBr}$, ${\rm Fe_2O_3})^{23-25}$ and nitrides (e.g. ${\rm C_3N_4}).^{26,27}$

Independent of the pathway for achieving electrified ammonia synthesis, nearly all routes use high-purity nitrogen as the reactant. Furthermore, most neglect the air separation unit when reporting energy efficiency. 24,28-32 Performing nitrogen catalysis in the presence of oxygen (e.g., in air) is nonideal. The presence of oxygen in the reactant mixture decreases the concentration of the reactant (N2), presenting mass-transfer-based challenges. Oxygen can also react with photogenerated charge carriers (electrons and holes) producing reactive oxygen species, thereby decreasing the conversion efficiency. 29,31,33 Oxygen can also react with the product (ammonia), decreasing the yield. Finally, the presence of ammonia, hydrogen, and oxygen is explosive, presenting safety challenges.³⁴ To date, only a few investigations have examined the photocatalytic activity of a photocatalyst in air. The most notable is when Hirakawa and colleagues examined rutile phase titania in air and nitrogen and reported a 65% decrease in yield when high-purity nitrogen was replaced by air.²³ Furthermore, one theoretical analysis suggests that the addition of dopants into oxides (cobalt, molybdenum, and vanadium) could aid in reducing oxygen adsorption, improving the photocatalytic nitrogen fixation activity.³

Here, we detail a technoeconomic analysis demonstrating the levelized cost of ammonia with and without air separation. We examine the cost of a photocatalytic nitrogen fixing system for various capital cost reactors and for various capital cost air separating units. We also examine the performance of a photocatalytic ammonia reactor with undoped and metal-doped ${\rm TiO_2}$ under aerobic and anaerobic conditions. Finally, we use transient photocurrent responses to examine the impact the oxygen reduction has in reducing system performance under aerobic conditions.

At large scales (>600 $\rm t_{N_2}/day$) cryogenic air separation cost 0.03–0.05 USD/kg $\rm N_2$ and produce nitrogen with a maximum purity of 99.999%. 36,37 This is advantageous for Haber–Bosch plants, which require ultra-high-purity nitrogen to preserve the catalyst and prevent ammonia oxidation. 38 However, large-scale cryogenic air separation can account for approximately 25% total cost of a whole Haber–Bosch plant. 33,39 The cost of producing nitrogen for a high-production-capacity (>2000 $\rm t_{N_2}/day$) synthesis facility (Haber–Bosch plant) is 0.03 USD/kg $\rm N_2$ (Figure 1).

At medium scales $(1-600~t_{\rm N_2}/{\rm day})$ pressure swing adsorption costs 0.05 USD/kg_{N_2} and produces nitrogen at a maximum purity of 99.99%. Finally, at small scale $(0.1-1~t_{\rm N_2}/{\rm day})$, membrane-based separations cost between 0.05 and \sim 0.1 USD/kg_{N_2} and produce nitrogen at a maximum purity of 99%. While the cost of membrane-based separations slightly exceeds the unit cost of cryogenic separations at high capacity, the cost of cryogenic separations at low capacity is approximately 5× more expensive than membranes. Complete elimination of separations could significantly reduce this cost, although there

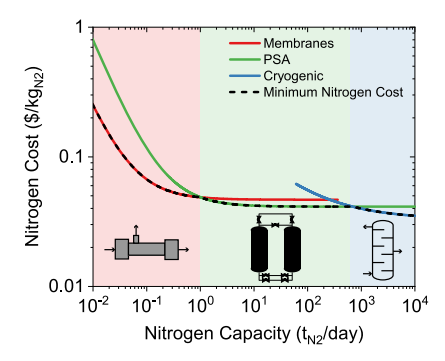


Figure 1. Nitrogen production cost $(C_{\rm N_2})$ for different air separation technologies and production capacities. Electricity cost assumed fixed at 0.06 USD/kWh. The black dashed line represents the minimum nitrogen cost at each production capacity.

still may be a need for air compression. Therefore, when designing photocatalytic reactors for ammonia synthesis, designing a catalyst that can withstand trace amounts of oxygen or air is essential to minimize cost.

The levelized cost of ammonia (LCOA) depends on the cost of air separation, the capital cost per unit area of the photochemical reactor (USD/m²), and the solar-to-ammonia efficiency. The air separation cost is estimated by the normalized cost of nitrogen per unit mass of produced nitrogen (USD/kg $_{\rm N_2}$). For a small-scale system, the cost of air separation will range from 0 USD/kg $_{\rm N_2}$ (no separations) to ~0.1 USD/kg $_{\rm N_2}$ (membrane separations) (see Supporting Information).

Unlike air separation units where the cost is well-known, cost estimates for different photochemical reactor designs are less clear, as few photocatalytic-based systems have been scaled up and deployed. Here, we estimate the cost for three photocatalytic reactor designs: particle suspension, fixed panel array, and solar concentrator array as 5, 20, and 100 USD/m². These capital estimates are obtained from a technoeconomic analysis of reactors for solar-to-hydrogen. 40 Understandably, the particle reactor architecture is the simplest and cheapest, whereas auxiliary components and manufacturing costs contribute to the higher cost for the fixed panel array and solar concentrator system. The solar-to-ammonia efficiency is defined as moles of ammonia multiplied by the free energy of ammonia generation from nitrogen and water (333.3 kJ/mol) per total solar energy input. The average solar flux to the ground is 200 W/m². The detailed calculations are shown in the SI.

With a low-cost photocatalytic reactor (slurry reactor: 5 USD/m²), the LCOA is highly dependent on the nitrogen production cost from the air separation unit $(C_{\rm N_2})$. This is demonstrated through the parabolic curvature of the isocost curves (Figure 2a). As the unit area capital cost increases (fixed panel array: 20 USD/m²), the LCOA increases, yet the impact the nitrogen production cost has on the LCOA decreases (Figure 2b). This is demonstrated through the flattening of the isocost curves with respect to the nitrogen production cost. Finally, at high-unit-area capital cost (concentrator array: 100 USD/m²), the LCOA is nearly independent of the nitrogen production cost (Figure 2c). This is demonstrated by the nearly horizontal isocost curves with respect to the nitrogen production cost. The red area in Figure 2 represents the conditions in which the LCOA exceeds 600 USD/t_{NH}, and

ACS Energy Letters http://pubs.acs.org/journal/aelccp Letter

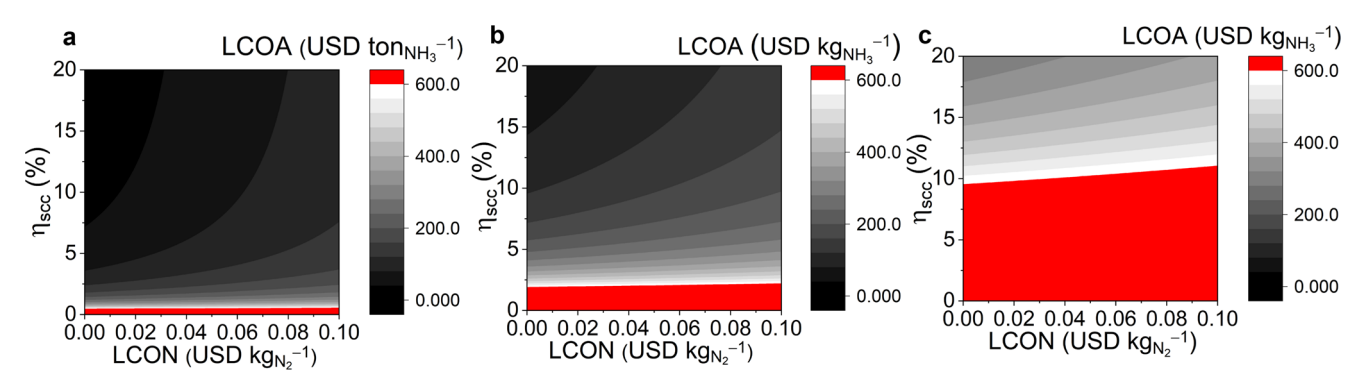


Figure 2. Levelized cost of ammonia for different photocatalytic reactor architectures. (a) Slurry reactor: 5 USD/m², (b) fixed panel reactor: 20 USD/m², and (c) concentrator array reactor: 100 USD/m². The red shaded area refers to our target LCOA (600 USD/t).

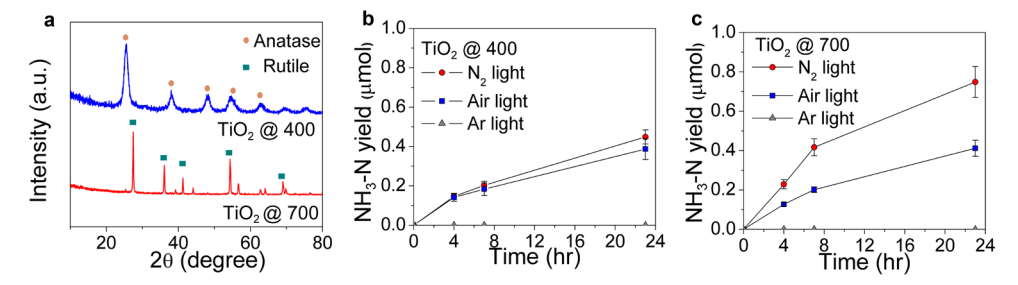


Figure 3. (a) XRD patterns of $TiO_2@400$ and $TiO_2@700$. (b) Time course for NH₃ production yields over $TiO_2@400$ and (c) $TiO_2@700$ under illumination (300 W, λ > 350 nm) in nitrogen and air environments.

thus demonstrates the case where the photocatalytic reactor would not reach a Haber-Bosch parity.

With a low-cost photocatalytic reactor (slurry reactor: 5 USD/m²), the required solar-to-ammonia efficiency to achieve costs slightly below 600 USD/t_{NH3} is 1%. While this competes with the Haber-Bosch process, it is envisioned that a distributed system must be cheaper than the Haber-Bosch process in reality due to the need for maintaince and other long-term costs. Thus, if the solar-to-ammonia efficiency is increased to 10%, the levelized cost of ammonia decreases to as low as 30 USD/ t_{NH_2} for the case of no air separation ($C_{N_2} = 0$) or aerobic nitrogen fixation. To put this into perspective, this is more than 10× less than the cost of fertilizer today. However, this cost increases to 110 USD/t_{NH3} when utilizing a membrane air separation system (0.1 USD/kg_{N_2}). This represents a 270% increase in the levelized cost of ammonia when moving from aerobic photocatalytic nitrogen reduction to anaerobic photocatalytic nitrogen reduction powered by membrane air separation.

As the unit area capital cost increases (fixed panel array: $20 \, \mathrm{USD/m^2}$) the required solar-to-ammonia efficiency to achieve an LCOA below 600 USD/ $t_{\mathrm{NH_3}}$ increases to approximately 2.5%. If the solar-to-ammonia efficiency is increased to 10%, the levelized cost of ammonia decreases to as low as 120 USD/ $t_{\mathrm{NH_3}}$ for the case of no air separation ($C_{\mathrm{N_2}}=0$) or aerobic nitrogen fixation. However, this cost increases to 200 USD/ $t_{\mathrm{NH_3}}$ when utilizing a membrane air separation system (0.1 USD/ $t_{\mathrm{NH_3}}$). This represents a 60% increase in the levelized cost of ammonia when moving from aerobic photocatalytic nitrogen reduction to anaerobic photocatalytic nitrogen reduction powered by membrane air separation.

Finally, at high-unit-area capital cost (concentrator array: $100~USD/m^2)$ the required solar-to-ammonia efficiency to achieve costs below $600~USD/t_{\rm NH_3}$ increases to 10%. With such high capital costs, the dependence of the LCOA on the nitrogen production cost decreases. For this reactor type operating at a solar-to-ammonia efficiency of 10%, an increase in the nitrogen production cost from 0 to $0.1~USD/kg_{\rm N_2}$ causes an increase in the LCOA from 580 to $660~USD/t_{\rm NH_3}$. This represents only a 14% increase in the levelized cost of ammonia when moving from aerobic photocatalytic nitrogen reduction to anaerobic photocatalytic nitrogen reduction powered by membrane air separation.

This analysis demonstrates that while air separation is expensive, the impact on the total system cost is accentuated for high-capital-cost reactors. With the growing movement to frugal and decentralized ammonia production devices where low-capital reactor architectures are preferred, removing air separation has a significant impact on the LCOA. As such, we next aim to demonstrate the impact aerobic conditions play on the activity of a photocatalyst.

Aerobic photocatalytic nitrogen fixation is ideal as it would enable the complete elimination of an air separation unit. However, the impacts oxygen has on deactivating the catalyst and/or oxidizing ammonia are unclear. On examination of the reaction kinetics, ammonia oxidation is unlikely to occur below 400 K if ammonia is the predominate form (Figure S1a). This occurs typically under alkaline conditions (pH > 10) in an aqueous phase reactor. The ammonia oxidation temperature further increases to 500 K if ammonia is in the ammonium form. This occurs in lower pH solutions (Figure S1b). Therefore, unlike the Haber–Bosch process, where trace amounts of oxygen can result in significant ammonia oxidation, this is unlikely to be a significant issue with ambient

ACS Energy Letters http://pubs.acs.org/journal/aelccp Letter

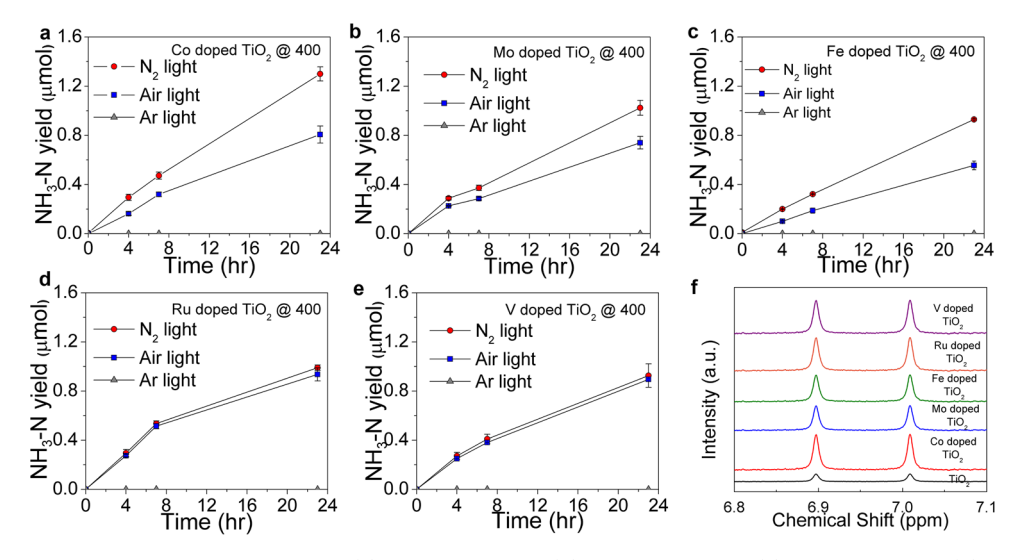


Figure 4. Time course ammonia production yield of (a) Co-doped TiO₂, (b) Mo-doped TiO₂, (c) Fe-doped TiO₂, (d) Ru-doped TiO₂, and (e) V-doped TiO₂ under nitrogen and air. (f) Isotope labeling ¹H NMR experiments of variously doped TiO₂.

temperature photocatalytic nitrogen fixation under aerobic conditions.

The photocatalytic activities of anatase (TiO2@400) and rutile (TiO₂@700) titania were measured in the presence of air, nitrogen, and argon (Figure 3). Under anaerobic conditions (nitrogen), the rutile phase (TiO₂@700) exhibited a \sim 48 \pm 20% higher rate of ammonia production than anatase titania (TiO₂@400) (Figure 3b,c). Under aerobic conditions (air), the rate of ammonia production declined for both anatase (TiO₂@400) and rutile (TiO₂@700) phases (Figure 3b,c). However, the performance decline for rutile (TiO₂@ 700) titania was more significant (\sim 52 \pm 17%) when compared to anatase (\sim 20 \pm 23%). Rutile phase titania has been shown to bind oxygen more strongly than the anatase TiO₂, which may have contributed to the reduced performance under aerobic conditions. 41 Furthermore, this performance decline in aerobic conditions aligned with prior investigations of titania in air. 42 Note that all experiments conducted under illumination with argon had negligible ammonia, suggesting that contamination did not contribute to the measured ammonia. The corresponding rates of ammonia produced by TiO_2 @700 under nitrogen and air are 0.06 \pm 0.02 and 0.03 \pm 0.01 μ mol hr⁻¹ (Figure S2). The corresponding rates of ammonia produced by TiO2@400 under nitrogen and air are 0.04 ± 0.003 and $0.027 \pm 0.008 \ \mu \text{mol hr}^{-1}$.

The insertion of metal dopants into the crystal lattice is widely examined as a means to increase the photocatalytic activity. The addition of another metal can aid activity through either disrupting the lattice structure, inducing active defects (e.g., vacancies), or serving as an active site. Here, we investigated five metal dopants (cobalt, molybdenum, iron, ruthenium, and vanadium). These metals were chosen because they are known as active catalysts for nitrogen reduction and were theorized to bind nitrogen in the presence of oxygen. ⁴³

All metal-doped titania samples calcined at 400 $^{\circ}$ C resulted in the formation of an anatase phase (Figure S3a). All metal-doped titania samples calcined at 700 $^{\circ}$ C resulted in the formation of a rutile phase (Figure S3b). This was consistent with the undoped titania (Figure 3a) where that calcined at 400 $^{\circ}$ C formed anatase phase titania and that calcined at 700 $^{\circ}$ C formed rutile phase titania. We also used ICP-MS to

confirm that the metal was successfully doped on the surface of various metal-doped titania (Table S3).

The ammonia yield for all metal-doped TiO_2 calcined at 400 °C in high-purity nitrogen was around ~2× greater than undoped $TiO_2@400$ (Figure S4a), with the rate of ammonia reaching between 0.067 ± 0.01 to 0.08 ± 0.006 . The ammonia yield for all metal-doped TiO_2 calcined at 700 °C in high-purity nitrogen was around ~2× less than undoped $TiO_2@700$ (Figure S4b).

We then conducted electron paramagnetic resonance (EPR) to provide insight into how the metal dopant altered the crystal structure. For instance, the emergence of undercoordinated Ti^{3+} ($g \approx 1.97$) and oxygen vacancies (O_v) ($g \approx 2.004$) is observerable. Undoped TiO₂@700 (rutile phase) had a greater Ti³⁺ and O₁₁ signal (Figure S5a) than undoped TiO₂@400 (anatase phase) (Figure S5b). This signifies that rutile phase titania (TiO₂@700) had a higher density of defects than anatase titania (TiO2@400). Therefore, the enhanced photocatalytic activity of undoped TiO2@700 may be attributed to the higher concentration of defects. This is consistent with a prior investigation.⁴² Conversely, for the metal-doped titania samples, the TiO₂@700 had more significant Ti³⁺ and O_v signals (Figure S5a) than the TiO₂@400 (Figure S5b). This again correlated with a higher nitrogen fixation activity. Similar trends also occur with XPS spectra in the Supporting Information (Figures S6 and S7).

Since the metal-doped TiO₂@400 had higher nitrogen reduction activity than undoped TiO2@700, we further investigated the activity under aerobic conditions and anaerobic conditions. Under aerobic conditions, the Co-, Mo-, and Fe-doped TiO₂@400 were lower (52, 41, and 48%) when compared to the anaerobic condition (Figure 4a-c). This is in part due to the favorable oxygen reduction reaction on iron, cobalt, and nickel oxides. 44,45 However, Ru- and Vdoped TiO₂@400 maintain similar ammonia production rates and total yield in aerobic and anaerobic conditions (Figure 4d,e). This may be in part due to the fact that RuO₂ exhibits favorable nitrogen reduction reaction activity.35 Meanwhile, vanadium is often stable and not easily oxidized by air and therefore could be able to maintain similar activities compared to pure nitrogen. We also conducted transient photocurrent responses in N2, Air and O2 to further explore the reason Ru and V elements on ${\rm TiO_2}$ could maintain similar ${\rm N_2}$ reduction activity under air in comparison to high-purity nitrogen (Figure S9). All catalysts operated in an argon environment (controls) with illumination had no ammonia being measured.

In all conditions, since the temperature was maintained at 28 $^{\circ}$ C, negligible levels of nitrate formed during the photocatalysis process when there is a trace amount of oxygen. ⁴⁶ Therefore, doping these two metals on TiO_2 could not only promote the photocatalytic nitrogen fixation but also maintain similar performance in air.

Isotope labeling experiments on undoped and variously doped ${\rm TiO_2}$ on ${}^1{\rm H}$ NMR by using ${}^{15}{\rm N_2}$ gas showed that the ammonia production yields on these five metal-doped titania samples are higher than undoped titania (Figure 4f). Similar trends on ${}^1{\rm H}$ NMR by using ${}^{14}{\rm N_2}$ gas are demonstrated in the Supporting Information (Figure S8a). The quantification of ammonia with ${}^{15}{\rm N_2}$ and ${}^{14}{\rm N_2}$ gases were comparable and differed by less than 10%. Furthermore, the ammonia concentrations obtained by ionic chromatography were similar to those obtained through NMR (Table S2).

The cost of an air separation unit is a critical bottleneck to decentralized ammonia production. A technoeconomic analysis demonstrates that through removing the air separation unit and the use of a low-capital photocatalytic reaction (slurry-based), the LCOA of a solar-driven fertilizer system is minimized and may drop below 100 USD/t. Moving away from anaerobic conditions will require catalysts that are stable, selectively bind nitrogen, and do not reduce oxygen. In particular, Ru- and V-doped TiO₂ were two promising materials that maintain similar nitrogen photocatalytic nitrogen reduction activity under aerobic and anaerobic conditions, whereas Co-, Mo-, and Fe-doped TiO₂ showed a significant (42 to 50%) decline in performance.

ASSOCIATED CONTENT

Supporting Information

The Supporting Information is available free of charge at https://pubs.acs.org/doi/10.1021/acsenergylett.1c02260.

Methods of air separation costs, ammonia oxidation analysis, ammonia production rate of anatase and rutile phase titania, XRD patterns of metal-doped titania samples, ammonia production rate of variously doped titania samples, ionic chromatography raw data of various metal-doped titania samples, calibration curve for ammonia on ionic chromatography and ¹H NMR, XPS data of various metal-doped titania samples, EPR spectra, and the trasient photocurrent response (PDF)

AUTHOR INFORMATION

Corresponding Author

Marta C. Hatzell — Woodruff School of Mechanical Engineering, Georgia Institute of Technology, Atlanta, Georgia 30332, United States; oorcid.org/0000-0002-5144-4969; Email: marta.hatzell@me.gatech.edu

Authors

Yu-Hsuan Liu – School of Civil and Environmental Engineering, Georgia Institute of Technology, Atlanta, Georgia 30332, United States

Carlos A. Fernández – Woodruff School of Mechanical Engineering, Georgia Institute of Technology, Atlanta, Georgia 30332, United States Sai A. Varanasi — Woodruff School of Mechanical Engineering, Georgia Institute of Technology, Atlanta, Georgia 30332, United States; Occid.org/0000-0003-4729-933X

Nhat Nguyen Bui — National High Magnetic Field Laboratory, Florida State University, Tallahassee, Florida 32310, United States

Likai Song – National High Magnetic Field Laboratory, Florida State University, Tallahassee, Florida 32310, United States

Complete contact information is available at: https://pubs.acs.org/10.1021/acsenergylett.1c02260

Notes

The authors declare no competing financial interest.

ACKNOWLEDGMENTS

This material is based upon work supported by the National Science Foundation under Grant Nos. 1846611 and 1933646. The National High Magnetic Field Laboratory is supported by NSF DMR 1644779 and the State of Florida.

REFERENCES

- (1) MacFarlane, D. R.; Cherepanov, P. V.; Choi, J.; Suryanto, B. H.R.; Hodgetts, R. Y.; Bakker, J. M.; Ferrero Vallana, F. M.; Simonov, A. N. A roadmap to the ammonia economy. *Joule* **2020**, *4*, 1186—1205.
- (2) Comer, B. M.; Medford, A. J. Analysis of Photocatalytic Nitrogen Fixation on Rutile TiO₂ (110). ACS Sustainable Chem. Eng. **2018**, 6, 4648–4660.
- (3) Comer, B. M.; Fuentes, P.; Dimkpa, C. O.; Liu, Y.-H.; Fernandez, C. A.; Arora, P.; Realff, M.; Singh, U.; Hatzell, M. C.; Medford, A. J. Prospects and Challenges for Solar Fertilizers. *Joule* **2019**, *3*, 1578–1605.
- (4) Suryanto, B. H.; Matuszek, K.; Choi, J.; Hodgetts, R. Y.; Du, H.-L.; Bakker, J. M.; Kang, C. S.; Cherepanov, P. V.; Simonov, A. N.; MacFarlane, D. R. Nitrogen reduction to ammonia at high efficiency and rates based on a phosphonium proton shuttle. *Science* **2021**, *372*, 1187–1191.
- (5) Fernandez, C. A.; Hortance, N. M.; Liu, Y.-H.; Lim, J.; Hatzell, K. B.; Hatzell, M. C. Opportunities for intermediate temperature renewable ammonia electrosynthesis. *J. Mater. Chem. A* **2020**, *8*, 15591–15606.
- (6) Fernandez, C. A.; Hatzell, M. C. Economic Considerations for Low-Temperature Electrochemical Ammonia Production: Achieving Haber—Bosch Parity. J. Electrochem. Soc. 2020, 167, 143504.
- (7) Yara Fertilizer Industry Handbook; Yara International, 2018.
- (8) Erisman, J. W.; Sutton, M. A.; Galloway, J.; Klimont, Z.; Winiwarter, W. How a century of ammonia synthesis changed the world. *Nat. Geosci.* **2008**, *1*, 636–639.
- (9) Foster, S. L.; Bakovic, S. I. P.; Duda, R. D.; Maheshwari, S.; Milton, R. D.; Minteer, S. D.; Janik, M. J.; Renner, J. N.; Greenlee, L. F. Catalysts for nitrogen reduction to ammonia. *Nat. Catal.* **2018**, *1*, 490–500.
- (10) Greenlee, L. F.; Renner, J. N.; Foster, S. L. The use of controls for consistent and accurate measurements of electrocatalytic ammonia synthesis from dinitrogen. *ACS Catal.* **2018**, *8*, 7820.
- (11) Wang, J.; Yu, L.; Hu, L.; Chen, G.; Xin, H.; Feng, X. Ambient ammonia synthesis via palladium-catalyzed electrohydrogenation of dinitrogen at low overpotential. *Nat. Commun.* **2018**, *9*, 1795.
- (12) Westhead, O.; Jervis, R.; Stephens, I. E. Is lithium the key for nitrogen electroreduction? *Science* **2021**, 372, 1149–1150.
- (13) Bagger, A.; Wan, H.; Stephens, I. E.; Rossmeisl, J. Role of Catalyst in Controlling N2 Reduction Selectivity: A Unified View of Nitrogenase and Solid Electrodes. ACS Catal. 2021, 11, 6596–6601.
- (14) Bao, D.; Zhang, Q.; Meng, F.-L.; Zhong, H.-X.; Shi, M.-M.; Zhang, Y.; Yan, J.-M.; Jiang, Q.; Zhang, X.-B. Electrochemical

- reduction of N2 under ambient conditions for artificial N2 fixation and renewable energy storage using N2/NH3 cycle. *Adv. Mater.* **2017**, 29, 1604799.
- (15) Cheng, H.; Ding, L.-X.; Chen, G.-F.; Zhang, L.; Xue, J.; Wang, H. Molybdenum carbide nanodots enable efficient electrocatalytic nitrogen fixation under ambient conditions. *Adv. Mater.* **2018**, *30*, 1803694.
- (16) Choi, J.; Suryanto, B. H. R.; Wang, D.; Du, H.-L.; Hodgetts, R. Y.; Ferrero Vallana, F. M.; MacFarlane, D. R.; Simonov, A. N. Identification and elimination of false positives in electrochemical nitrogen reduction studies. *Nat. Commun.* **2020**, *11*, 5546.
- (17) Song, Y.; Johnson, D.; Peng, R.; Hensley, D. K.; Bonnesen, P. V.; Liang, L.; Huang, J.; Yang, F.; Zhang, F.; Qiao, R.; et al. A physical catalyst for the electrolysis of nitrogen to ammonia. *Sci. Adv.* **2018**, *4*, No. e1700336.
- (18) Lim, J.; Liu, C.-Y.; Park, J.; Liu, Y.-H.; Senftle, T. P.; Lee, S. W.; Hatzell, M. C. Structure Sensitivity of Pd Facets for Enhanced Electrochemical Nitrate Reduction to Ammonia. *ACS Catal.* **2021**, *11*, 7568–7577.
- (19) Hawtof, R.; Ghosh, S.; Guarr, E.; Xu, C.; Mohan Sankaran, R.; Renner, J. N. Catalyst-free, highly selective synthesis of ammonia from nitrogen and water by a plasma electrolytic system. *Sci. Adv.* **2019**, *5*, No. eaat5778.
- (20) Gorbanev, Y.; Vervloessem, E.; Nikiforov, A.; Bogaerts, A. Nitrogen fixation with water vapor by nonequilibrium plasma: toward sustainable ammonia production. *ACS Sustainable Chem. Eng.* **2020**, *8*, 2996–3004.
- (21) Tricker, A. W.; Hebisch, K. L.; Buchmann, M.; Liu, Y.-H.; Rose, M.; Stavitski, E.; Medford, A. J.; Hatzell, M. C.; Sievers, C. Mechanocatalytic Ammonia Synthesis over TiN in Transient Microenvironments. *ACS Energy Letters* **2020**, *5*, 3362–3367.
- (22) Medford, A. J.; Hatzell, M. C. Photon-driven nitrogen fixation: current progress, thermodynamic considerations, and future outlook. *ACS Catal.* **2017**, *7*, 2624–2643.
- (23) Hirakawa, H.; Hashimoto, M.; Shiraishi, Y.; Hirai, T. Photocatalytic Conversion of Nitrogen to Ammonia with Water on Surface Oxygen Vacancies of Titanium Dioxide. *J. Am. Chem. Soc.* **2017**, *139*, 10929–10936.
- (24) Li, H.; Shang, J.; Ai, Z.; Zhang, L. Efficient visible light nitrogen fixation with BiOBr nanosheets of oxygen vacancies on the exposed {001} facets. *J. Am. Chem. Soc.* **2015**, *137*, 6393–6399.
- (25) Lashgari, M.; Zeinalkhani, P. Photocatalytic N2 conversion to ammonia using efficient nanostructured solar-energy-materials in aqueous media: A novel hydrogenation strategy and basic understanding of the phenomenon. *Appl. Catal., A* **2017**, *529*, 91–97.
- (26) Liang, C.; Niu, H.-Y.; Guo, H.; Niu, C.-G.; Huang, D.-W.; Yang, Y.-Y.; Liu, H.-Y.; Shao, B.-B.; Feng, H.-P. Insight into photocatalytic nitrogen fixation on graphitic carbon nitride: Defect-dopant strategy of nitrogen defect and boron dopant. *Chem. Eng. J.* **2020**, *396*, 125395.
- (27) Shiraishi, Y.; Shiota, S.; Kofuji, Y.; Hashimoto, M.; Chishiro, K.; Hirakawa, H.; Tanaka, S.; Ichikawa, S.; Hirai, T. Nitrogen fixation with water on carbon-nitride-based metal-free photocatalysts with 0.1% solar-to-ammonia Energy Conversion Efficiency. ACS Appl. Energy Mater. 2018, 1, 4169–4177.
- (28) Zhao, Y.; Zhao, Y.; Shi, R.; Wang, B.; Waterhouse, G. I.; Wu, L.-Z.; Tung, C.-H.; Zhang, T. Tuning oxygen vacancies in ultrathin TiO2 nanosheets to boost photocatalytic nitrogen fixation up to 700 nm. *Adv. Mater.* **2019**, *31*, 1806482.
- (29) Ye, L.; Han, C.; Ma, Z.; Leng, Y.; Li, J.; Ji, X.; Bi, D.; Xie, H.; Huang, Z. Ni2P loading on Cd0. 5Zn0. SS solid solution for exceptional photocatalytic nitrogen fixation under visible light. *Chem. Eng. J.* 2017, 307, 311–318.
- (30) Fang, Y.; Xue, Y.; Hui, L.; Yu, H.; Li, Y. Graphdiyne@ Janus magnetite for photocatalytic nitrogen fixation. *Angew. Chem.* **2021**, 133, 3207–3211.
- (31) Huang, H.; Wang, X.-S.; Philo, D.; Ichihara, F.; Song, H.; Li, Y.; Li, D.; Qiu, T.; Wang, S.; Ye, J. Toward visible-light-assisted

- photocatalytic nitrogen fixation: A titanium metal organic framework with functionalized ligands. *Appl. Catal., B* **2020**, *267*, 118686.
- (32) Sun, B.; Liang, Z.; Qian, Y.; Xu, X.; Han, Y.; Tian, J. Sulfur vacancy-rich O-doped 1T-MoS2 nanosheets for exceptional photocatalytic nitrogen fixation over CdS. ACS Appl. Mater. Interfaces 2020, 12, 7257–7269.
- (33) Comer, B. M.; Liu, Y.-H.; Dixit, M. B.; Hatzell, K. B.; Ye, Y.; Crumlin, E. J.; Hatzell, M. C.; Medford, A. J. The role of adventitious carbon in photo-catalytic nitrogen fixation by titania. *J. Am. Chem. Soc.* **2018**, *140*, 15157–15160.
- (34) Silverman, A. Le Chatelier and the synthesis of ammonia. J. Chem. Educ. 1938, 15, 289.
- (35) Hoskuldsson, A. B.; Abghoui, Y.; Gunnarsdottir, A. B.; Skulason, E. Computational screening of rutile oxides for electrochemical ammonia formation. *ACS Sustainable Chem. Eng.* **2017**, *5*, 10327–10333.
- (36) Castle, W. Air separation and liquefaction: recent developments and prospects for the beginning of the new millennium. *Int. J. Refrig.* **2002**, *25*, 158–172.
- (37) Smith, A.; Klosek, J. A review of air separation technologies and their integration with energy conversion processes. *Fuel Process. Technol.* **2001**, *70*, 115–134.
- (38) Smith, C.; Hill, A. K.; Torrente-Murciano, L. Current and future role of Haber–Bosch ammonia in a carbon-free energy landscape. *Energy Environ. Sci.* **2020**, *13*, 331–344.
- (39) Bartels, J. R. A feasibility study of implementing an Ammonia Economy, M.S. Thesis. Iowa State University, 2008.
- (40) Shaner, M. R.; Atwater, H. A.; Lewis, N. S.; McFarland, E. W. A comparative technoeconomic analysis of renewable hydrogen production using solar energy. *Energy Environ. Sci.* **2016**, *9*, 2354–2371.
- (41) Buchalska, M.; Kobielusz, M.; Matuszek, A.; Pacia, M.; Wojtyła, S.; Macyk, W. On oxygen activation at rutile-and anatase-TiO2. ACS Catal. 2015, 5, 7424–7431.
- (42) Hirakawa, H.; Hashimoto, M.; Shiraishi, Y.; Hirai, T. Photocatalytic conversion of nitrogen to ammonia with water on surface oxygen vacancies of titanium dioxide. *J. Am. Chem. Soc.* **2017**, 139, 10929–10936.
- (43) Comer, B. M.; Lenk, M. H.; Rajanala, A. P.; Flynn, E. L.; Medford, A. J. Computational Study of Transition-Metal Substitutions in Rutile TiO 2 (110) for Photoelectrocatalytic Ammonia Synthesis. *Catal. Lett.* **2021**, *151*, 1142–1154.
- (44) Wang, Y.; Li, J.; Wei, Z. Transition-metal-oxide-based catalysts for the oxygen reduction reaction. *J. Mater. Chem. A* **2018**, *6*, 8194–8209
- (45) Xue, Y.; Sun, S.; Wang, Q.; Dong, Z.; Liu, Z. Transition metal oxide-based oxygen reduction reaction electrocatalysts for energy conversion systems with aqueous electrolytes. *J. Mater. Chem. A* **2018**, *6*, 10595–10626.
- (46) Linnik, O.; Kisch, H. On the mechanism of nitrogen photofixation at nanostructured iron titanate films. *Photochem. Photobiol. Sci.* **2006**, *5*, 938–942.